Photometric-based recovery of illuminant-free color images using a red-green-blue digital camera

Juan Luis Nieves
Clara Plata
Eva M. Valero
Javier Romero

Photometric-based recovery of illuminant-free color images using a red-green-blue digital camera

Juan Luis Nieves
Clara Plata
Eva M. Valero
Javier Romero
Universidad de Granada
Departamento de Óptica
Facultad de Ciencias
18071-Granada, Spain
E-mail: jnieves@ugr.es

Abstract. Albedo estimation has traditionally been used to make computational simulations of real objects under different conditions, but as yet no device is capable of measuring albedo directly. The aim of this work is to introduce a photometric-based color imaging framework that can estimate albedo and can reproduce the appearance both indoors and outdoors of images under different lights and illumination geometry. Using a calibration sample set composed of chips made of the same material but different colors and textures, we compare two photometric-stereo techniques, one of them avoiding the effect of shadows and highlights in the image and the other ignoring this constraint. We combined a photometric-stereo technique and a color-estimation algorithm that directly relates the camera sensor outputs with the albedo values. The proposed method can produce illuminant-free images with good color accuracy when a three-channel red-green-blue (RGB) digital camera is used, even outdoors under solar illumination. © *2012 Society of Photo-Optical Instrumentation Engineers (SPIE).* [DOI: 10.1117/1.OE.51.1.013201]

Subject terms: color; spectral reflectance; photometric-stereo; illuminant.

Paper 110307 received Mar. 29, 2011; revised manuscript received Jul. 20, 2011; accepted for publication Nov. 7, 2011; published online Feb. 6, 2012.

1 Introduction

Our visual system allows us to distinguish elements such as color, texture, and surface shape, and our brains use this information to recognize objects under different lighting and observation conditions. Computational vision uses imaging devices to simulate the way the human visual system analyzes color images. Reproducing color appearance in color-based image displays depends on several factors such as the imaging device itself, the geometry of the lighting conditions, and the surface properties of the objects in question. When dealing with textured objects these factors become more evident; for example, the position of the camera and the object must be kept fixed because the color appearance of the object can change with the direction of illumination, which can cause a problem for object characterization. Thus, extracting information from textured images independently of lighting and imaging geometries poses a challenge for many computational vision systems. The use of the albedo rather than raw sensor response data can help to solve this issue. Albedo is usually defined as the ratio of scattered flux to that scattered and absorbed by a monodisperse or relatively uniform suspension, i.e., the ratio of flux scattered to the quantity of incident flux.[1] As opposed to intensity, albedo does not depend on the illumination conditions, and has been used in computer graphics to derive illuminant-invariant properties.[2] But the light reflected from a surface depends on the surface's spectral characteristics, the illumination geometry, the spectral content of the incident light, the viewing direction, and the roughness of the surface. This means that albedo recovery should not only be insensitive to the intensity of illumination but also to spectral changes in the reflected light.

Photometric stereo algorithms have long been used to estimate 3D surface properties of objects.[3] The photometric stereo approach is based on the fact that image intensity depends on the orientation of the surface with regard to the source of the illumination and its spectral reflectance. If several images are taken from the same point of view but with different lighting directions, any variation in pixel radiance in these images must be due to changes in the relative positions of the light and the surface. In recent years different photometric stereo techniques have been proposed to recover the normal vectors to the surface and albedo from digital images.[3–14] A common strategy of all these techniques is to estimate surface information either by measuring distances directly or by measuring parameters calculated from images of the illuminated objects.[7,15] Both approaches usually assume that objects exhibit Lambertian behavior in the underlying reflectance phenomenon, i.e., just before the acquisition process, all surfaces show the same radiance regardless of the illumination geometry. In computer graphics this means that objects reflect light diffusely in all directions and neither highlights nor shadows are present in the rendered images. Real objects are usually quite far from being Lambertian, and this means that photometric stereo algorithms may fail when used to recover surface normals and albedo in real-world scenes. Therefore several authors have developed different approaches to avoid these non-Lambertian behaviors and applied the algorithms in a more realistic environment, either indoors or outdoors.[8,10]

Most photometric stereo techniques only take into account gray-scale images, although some papers do describe the extension of this method to color images.[5,9,11] Most of these techniques are based on the fact that information concerning the color image of a Lambertian surface illuminated by a single light source is irrelevant because the photometric equations for individual color bands are linearly

dependent. An efficient way of exploiting this irrelevance is to use a conventional photometric stereo method relying on a single color image of a Lambertian surface under complex lighting conditions rather than three gray-scale images.[5] One interesting approach to avoid the use of multiple images is the one recently proposed by Bringier et al.[13] They obtained a surface-height map from an image using just one red-green-blue (RGB) color-image acquisition. Each color-image component (red, green, and blue) replaces gray images in the photometric approach. Their indoor results show that 3D surface information can be obtained for textured objects. Although the technique is easy to implement and not very expensive, it is based on the Lambertian model and so it is difficult to obtain perfect channel isolation with a single camera.

All of the methods described above are quite straightforward but are based solely on a RGB color description of images (i.e., three camera sensor responses or digital RGB values for each pixel). Recently other approaches have been proposed[11,12] to include the spectral reflectance properties of surfaces in the photometric-stereo analysis. Plata et al.[11] developed a spectral-based photometric-stereo algorithm to estimate the spectral reflectance of textured surfaces using a RGB digital camera. For economy and design convenience the device used only three color channels but the spectral information derived allowed image analysis and synthesis, even for rough-textured surfaces lit by spectrally different illumination sources from different directions. In addition the use of albedo for each channel instead of direct RGB information avoided any shadows or highlights that might bias the results. Nevertheless, it was difficult to assess the accuracy of such a system and the information was incomplete because the metrics for evaluating its quality were restricted to RGB values alone and no solution was offered for natural illumination conditions, where the appearance of color images can change as the sun moves across the sky.

How to estimate the albedo of color images reliably using the minimum number of color channels is a very important issue that has not been properly analyzed to date. In this paper we propose a photometric-based color-imaging framework to reproduce the color appearance of indoor and outdoor images under different lighting and illumination geometry. We combine a photometric-stereo technique and a color-estimation algorithm to directly relate the camera-sensor outputs and the albedo values. We used the system outdoors to prove that our photometric-stereo-based technique was a practical and easy way of testing albedo recovery without complex devices and/or strategies. Nowadays the applications are manifold: in the field of art and archiving in museums, where people demand virtual access to the arts catalog as though they were physically within the real illuminated room, and also in archaeology, where virtual reality can reproduce the color appearance of art works under different illumination conditions.

2 Method

Photometric stereo techniques have been used extensively to recover normal vectors and albedo in black and white (b/w) images. Two assumptions are usually made in the photometric stereo approach.[3,4] The surface is not perfectly smooth and is composed of microfacets, which have normal vectors that are distributed throughout the normal vector of the approximately smooth surface, and the surface is lit from a single source. All these methods start from the constraint of Lambertian surfaces, i.e., surfaces that present the same radiance in all directions of illumination. The surface can be described by a 2D height function, $z = S(x, y)$, and we can define the gradient components for every point of the surface as

$$p(x, y) = \frac{\partial S(x, y)}{\partial x}, \quad q(x, y) = \frac{\partial S(x, y)}{\partial y}, \quad (1)$$

and the normal unit vector $\mathbf{N}$ as

$$\mathbf{N} = \frac{1}{\sqrt{p^2 + q^2 + 1}} (p, q, -1)^T, \quad (2)$$

where T denotes the transpose of the vector. There are several complex ways of extending photometric stereo to color images[5,9,10] but in this work we will simply apply the above formulation to each color plane of our images, i.e., taking the R, G, B channels to be independent b/w channels. This method has a very low computational cost and has provided very good results.[11]

Thus, assuming that a monochrome camera (i.e., with just one sensor) collects the light reflected by a surface (Fig. 1(a)), we can model the surface normals, the albedo, and the image irradiance at a pixel x using the equation

$$I^x = \rho^x (\mathbf{L} \cdot \mathbf{N}^T)^x, \quad (3)$$

where I^x represents the camera outputs at pixel x, ρ^x is the albedo (i.e., the coefficient that represents the quantity of light reflected to the camera) at that point, $\mathbf{L}$ is the unit vector pointing at the light source, $\mathbf{N}$ is the unit vector normal to the surface, and $(\cdot)$ represents the inner product of two vectors. The aim of any photometric-stereo algorithm is to obtain a 3D reconstruction of an object's surface from Eq. (3) by estimating the normals and albedo using different captured images of the same object under a minimum of three different angles of illumination (Fig. 1(b)).[3] After illuminating the surface with each of those three lights, the corresponding radiances at any pixel will be given as

$$I_k^x = \rho^x (\mathbf{L}_k \cdot \mathbf{N}^T)^x, \quad (4)$$

where $k = 1, 2, 3$ represents the minimum of three illuminant directions. If the pixel radiances and the light vectors are stacked row-wise to rewrite Eq. (4) in a matrix form, and the three light directions $\mathbf{L}_k$ do not lie on the same plane, both the normals and the albedo can be estimated by solving

$$(\mathbf{L}^{-1}\mathbf{I})^x = \rho^x \mathbf{N}^x, \quad (5)$$

where $\mathbf{L}^{-1}$ now represents the inverse of the "intensity matrix" (each row of this matrix represents the pixel in the kth image).[11] In the above equations, controlling the lighting conditions is very important for the accuracy of the algorithm. It is essential to avoid ambient light and to keep the incident light intensity the same for the different directions of illumination, which can be achieved by keeping the distance between the light source and the object constant.
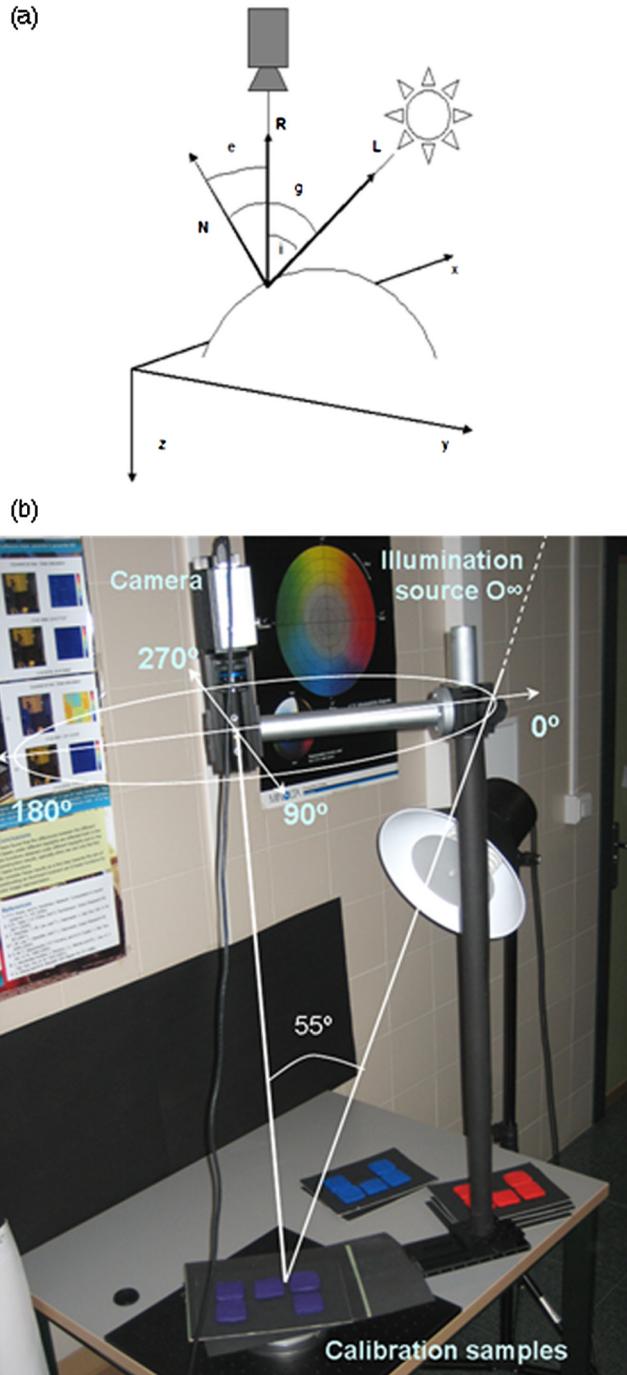
Fig. 1 (a) Definition of the important vectors and reflectance angles: R, viewer vector; L, illuminant vector; N, normal vector; i, incident angle; e, emittance angle; g, phase angle. (b) General view of the image capture of the same object under a minimum of three different angles of illumination and samples during calibration. The source of illumination was outside the frame of this picture.

2.1 Color Albedo Recovery

The color of an object depends on the spectral reflectance properties of its surface and the spectral power distribution (SPD) of the light that illuminates it.[15] Thus, when a linear color-acquisition system captures the radiance coming from a surface, the digital response of the sensor at a pixel (for simplicity's sake the pixel x notation used previously will be dropped in what follows) can be modeled as

$$Q^i = \int_\lambda e(\lambda) r(\lambda) s^i(\lambda) \mathrm{d}\lambda + \sigma^i, \qquad (6)$$

where Q_i is the ith sensor response, s^i is the ith spectral sensitivity of the camera (e.g., the spectral responsivities R, G, and B in the case of a trichromatic digital camera), e is the SPD of the illumination, r is the spectral reflectance of the object point, and the scalar σ^i models the noise in the ith channel. In this work the integral is evaluated within the wavelength λ range of [400,700] nm.

Here we propose a color albedo recovery based on the so-called "four-source photometric stereo."[10] Our proposal consists of applying the gray four-source photometric algorithm to each color channel (RGB sensor values) in a separate way, thus deriving three albedo values and three normal vectors for each pixel and combining Eqs. (4) and (6) as

$$\rho_k^i (\mathbf{L}_k \cdot \mathbf{N}^T) = \int_\lambda e_k(\lambda) r(\lambda) s^i(\lambda) \mathrm{d}\lambda + \sigma^i, \qquad (7)$$

where now $k = 1, 2, 3, 4$, and represents the number of light directions used to estimate the albedo and normals for each ith color channel. This implies solving

$$\mathbf{L}^{-1} \mathbf{Q}^i = \rho^i \mathbf{N}. \qquad (8)$$

The model considered so far assumes that surfaces behave in a Lambertian manner but if this assumption proves to be false will lead to unreliable results. To avoid this problem our strategy is to detect troublesome irradiance values in the image captured from the four different illuminant directions (i.e., those coming from shadows and highlights or those representative of non-Lambertian behavior).

But what happens if we detect more than one troublesome source of irradiance in the quadruplet of sensor responses for each channel and the four illuminant directions? This could lead to unsatisfactory results because at least three values are needed to apply photometric stereo and we cannot simply remove all of them. We have used two approaches to solve this problem: the first—uncorrected algorithm—presumes that all four pixels conform to Lambertian behavior and combines the four irradiances in four possible ways before averaging out the results for all the pixels in the image.[12] The second algorithm—corrected algorithm—addresses irradiances that might behave as non-Lambertian and acts according to the following procedure:

1. For each pixel x, the average of the four irradiances $\mathbf{I}^x = (I_1^x, I_2^x, I_3^x, I_4^x)$ is calculated as

$$I_{\mathrm{mean}}^x = \frac{\sum_{i=1}^4 I_i^x}{4}. \qquad (9)$$

2. To determine departure from the mean, the difference between I_{mean}^x and the maximum and minimum values of the irradiance $\mathbf{I}^x$ is estimated as

$$\mathbf{Mm}^x = [\max(\mathbf{I}^x) - I_{\mathrm{mean}}^x, I_{\mathrm{mean}}^x - \min(\mathbf{I}^x)]. \qquad (10)$$

3. A selection process begins by analyzing the vector $\mathbf{Mm}^x$ to choose the valid irradiance values and proceeds on the basis of one of the following conditions:

i. If the maximum value of $\mathbf{Mm}^x$ is the first element, i.e., $[\max(\mathbf{I}^x) - I_{\text{mean}}^x > I_{\text{mean}}^x - \min(\mathbf{I}^x)]$, it means that a highlighted pixel appears in the quadruplet and thus only the three lowest values of $\mathbf{I}^x$ will be used.

ii. If the maximum value of $\mathbf{Mm}^x$ is the second element, i.e., $[\max(\mathbf{I}^x) - I_{\text{mean}}^x < I_{\text{mean}}^x - \min(\mathbf{I}^x)]$, it means that a shadowed pixel appears in the quadruplet and thus only the three highest values of $\mathbf{I}^x$ will be considered.

iii. If the values of $\mathbf{Mm}^x$ are similar, i.e., $[\max(\mathbf{I}^x) - I_{\text{mean}}^x] \simeq [I_{\text{mean}}^x - \min(\mathbf{I}^x)]$ considering a 2% uncertainty in this estimate, there are two possibilities: either all four irradiances may behave in a Lambertian way and will be very similar (no shadowed or highlighted pixels at all) or two troublesome pixels may appear as either two shadows or two highlights. The strategy followed in these two cases is the same and is based on recovering albedo and normal vectors from the four possible combinations of three irradiances prior to the average results.

2.2 Image Dataset

Calibrating a device that allows albedo recovery is always a difficult task because few commercial devices are capable of measuring it.[16] Therefore, no reference values exist for comparison and many computational approaches try to avoid this issue simply by visually inspecting the rendered images. We built a set of calibration samples to solve this problem and prepared suitable targets to evaluate the accuracy of recovered albedos.[12,17] The color set comprised chip sets of seven different colors (pale pink, yellow, orange, red, green, blue, and purple), each composed of five chips made of the same material (polymer clay). All the samples were the same color but had different textures: flat or untextured surface, irregular, regular in one direction, concave, and convex. Figure 2 shows the molds we used to build the samples, made with the same material as the calibration samples.

The design of the calibration samples provides a way to assess the recovered albedo from a captured image. The errors in recovered albedo from the flat surface are minimal, since in this case the absence of textures allows us to obtain a perfectly smooth albedo.[12] The troublesome pixels do not occur because of the absence of highlights and shadows. Thus, the estimated albedo from the flat chip of each sample can be used as a reference to assess the accuracy of albedo recovery by comparing the estimated albedos from other textured chips with the corresponding reference albedo. The quality of the recovery is related to the similarity between the
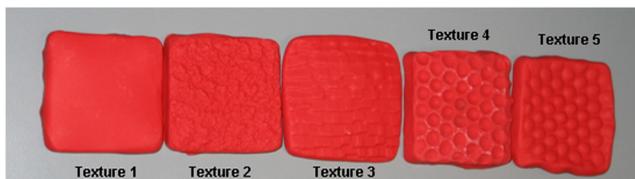

Fig. 2 Molds used in the fabrication of the calibration samples. The texture labeled as 1 corresponds to a uniform flat surface; textures 2 and 3 simulate random textured surfaces, and textures 4 and 5 are concave and convex textured surfaces, respectively.

recovered and reference albedo values and in this way we have assessed the two color photometric stereo algorithms presented in the previous section.

3 Results

To compare the estimated and reference albedos we used the relative albedo (RA) in the calibration experiment (i.e., using the set of calibration samples) expressed as

$$\text{RA} = \frac{|\rho_r - \rho_e|}{\frac{1}{2}|\rho_r| \cdot |\rho_e|} \times 100, \tag{11}$$

where ρ_r and ρ_e are the albedo values to compare (note that we are working with RGB images and these albedo values are three component vectors), $|\cdot|$ represents the modulus of a vector and $(\cdot)$ is the scalar product between vectors. From Eq. (7) it is easy to see that the far-right term of that equation represents the digital RGB values.

In addition, to quantify the quality of the image rendering results we used the RGB error ($\text{RGB}e_x$) at pixel x, the RGB relative error ($\text{RGB}r_x$), the angle error (AE), and the usual CIELab color difference (ΔE_{Lab}); all the metrics were calculated at each pixel. The $\text{RGB}e_x$ is defined as

$$\text{RGB}e_x = \sqrt{\frac{1}{3}(\Delta R_x^2 + \Delta G_x^2 + \Delta B_x^2)}, \tag{12}$$

where ΔR_x, ΔG_x and ΔB_x are the pixel-by-pixel differences for the three channels; accordingly the $\text{RGB}r_x$ is determined as

$$\text{RGB}r_x = \frac{|\mathbf{Q}_i - \mathbf{Q}_j|}{\frac{1}{2}|\mathbf{Q}_i| \cdot |\mathbf{Q}_j|} \times 100, \tag{13}$$

where $\mathbf{Q}_i$ and $\mathbf{Q}_j$ are the two RGB vectors at pixel x to compare, and the AE can thus be calculated as

$$\text{AE}_x = \arccos(\mathbf{Q}_i \cdot \mathbf{Q}_j). \tag{14}$$

CIELab color differences were obtained using the tristimulus values calculated from the RGB values of a white patch captured under the same illuminant as the samples as reference.[11]

3.1 Indoor Calibration Results

Images were captured with an RGB Retiga 1300 CCD camera with 12 bit intensity range per channel (QImaging, Canada) and fitted with a LINOS MeVis-C lens with a fixed 5.6 aperture and focal length of 25 mm. For each image we captured an associated black image and a white reference to compensate for the noise and possible spatial heterogeneities, respectively. The set-up allows the camera-sample pair to rotate together around the z axis with the relative position between the camera and the sample always fixed [see Fig. 1(b)]. In this way, by fixing one lamp it is possible to capture the sample under different illumination directions simply by rotating the sample and the camera. Additional details about the device can be found in reference number;[11] the main difference from the previous experiment is that here we directly relate digital RGB values and the albedo instead of first estimating the spectral reflectance function of the imaged surfaces. The calibration

samples were captured using a fluorescent lamp (a Bowens BW-3320 Trilite fluorescent daylight-type lamp)[18] as the illumination source. For acceptable photometric-stereo results the choice of the elevation and the azimuth angles for the ith source is not arbitrary. Four images were captured for each sample using a fixed elevation angle of the illumination source of 55 deg in all cases, and azimuth angles of 0, 90, 180 and 270 deg, thus ensuring that none of three illumination vectors lies in the same plane.[10]

As the flat surface (texture 1 in Fig. 2) is the simplest textured surface, the albedo recovered from it using different methods must be very similar. We averaged the pixel-by-pixel albedo values obtained along each flat surface and used this value as the reference albedo. Subsequently we compared reference albedo values, which were obtained from the seven flat samples, with both the uncorrected and corrected algorithms. We found a RA value of only 0.0543%, which means that the reference albedos deriving from the two methods were quite similar. Note that in this case it is not possible to use alternative colorimetric metrics (e.g., CIELab color difference) because we are not dealing with RGB values. The minimum RA value was 0.0001%, which was obtained for the flat green sample, and the maximum was 0.3642%, which was obtained for the flat purple sample.

Finding such similar reference albedos with both methods is a good starting point for calibrating the possibilities of the method. Thus the next step was to compare pixel by pixel the albedo recovered for the other non-flat color textures with the reference albedo of the same color. We analyzed the results in two different ways. Firstly, Table 1 shows the mean, median, and 95th-percentile results for each calibration sample, i.e., considering each color separately. The results obtained using the corrected algorithm were lower than those obtained with the uncorrected approach; the exceptions were the pale pink sample (mean RA of 9.8% and 10.6% for the uncorrected and the corrected algorithms, respectively) and the yellow sample (mean RA of 4.9% and 5.4% for the uncorrected and corrected algorithms, respectively). But the results shown in Table 2 as a function of surface texture suggest that the corrected algorithm produced better results than the uncorrected one. The best results were

Table 2 RA results obtained for the calibration samples classified by texture classes and the algorithm tested (P95 means the 95th percentile).

Texture	Uncorrected			Corrected		
	Mean	Median	P95	Mean	Median	P95
1	2.2	1.4	7.2	2.0	1.5	5.2
2	5.3	4.3	13.0	5.1	4.1	12.7
3	7.3	6.2	18.0	6.3	5.2	15.8
4	6.4	5.4	15.0	5.7	4.4	15.1
5	7.7	6.7	17.0	6.7	5.3	16.5

obviously for texture 1 because that texture was the flat surface, the average albedo of which was used as the reference albedo. An ANOVA statistical test showed that the performance depended on the algorithm used and showed significant differences ($p < 0.0001$) for the two factors considered: the color and the texture factors. Average results for the RA, for all the calibration samples and textures, were 5.8% (median of 4.4%) and 5.2% (median of 3.8%) for the uncorrected and the corrected algorithms, respectively.

Figure 3 shows examples of the recoveries for the convex purple and the concave pink calibration samples. The images in the first column are real captures of the samples under a lighting geometry of 55 deg elevation and 0 deg azimuth. The second and third columns are the illuminant-free images (e.g., albedo images) recovered with the uncorrected and corrected algorithms. The albedo images in the last column were smoother than the surface details in the originals. The visual significance of the examples is illustrated in the RGB errors shown in Fig. 4, where the average results suggest very good albedo recoveries for the corrected rendering algorithm and the whole set of calibration surfaces. The average RGBr_x is 3.7, which decreases to 2.9 when the median is taken into account. These values correspond to AE values of 0.78 and 0.57, respectively.
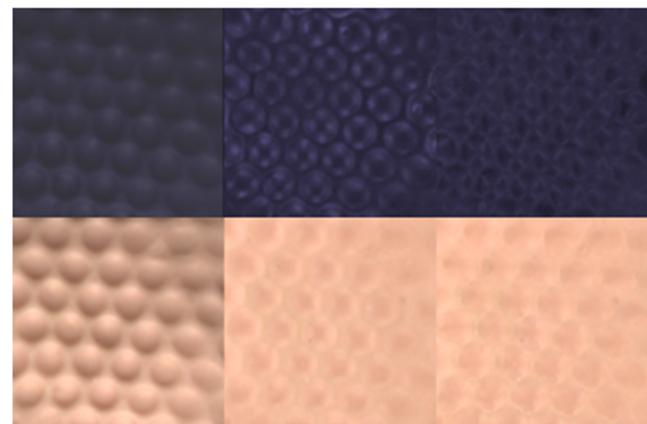
Table 1 RA results obtained for the calibration samples classified by color classes and the algorithm tested (P95 means the 95th percentile).

	Uncorrected			Corrected		
	Mean	Median	P95	Mean	Median	P95
Pale pink	9.8	10.7	18.4	10.6	11.6	19.1
Yellow	4.9	4.3	10.7	5.4	5.0	11.7
Orange	3.7	2.6	10.2	2.9	2.2	7.8
Red	3.9	3.1	10.2	3.4	2.7	8.6
Green	5.7	4.1	15.2	4.0	3.4	9.3
Blue	4.6	3.3	12.8	4.1	3.1	11.0
Purple	7.9	6.3	19.7	5.6	4.9	12.3

Fig. 3 Close-up view of the albedo recovery for the purple concave (upper row) and pink convex (lower row) calibration samples. The original surface is shown in the column on the left and the albedo recoveries are shown in the column on the far right for the uncorrected algorithm (central column) and the corrected one (right-hand column).
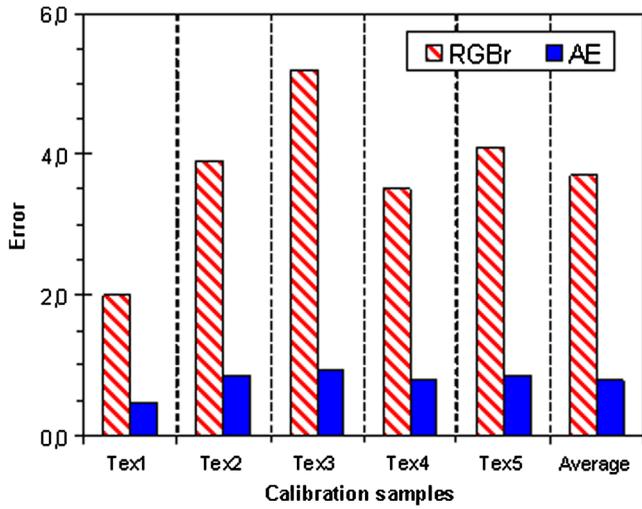
Fig. 4 RGB relative error (RGBr) and angle error (AE) obtained with the corrected algorithm for each textured sample. The last two bars are the average values for the whole calibration set.

3.2 Color Albedo Recovery Outdoors

It is straightforward to control the geometry of illumination for indoor environments. Nevertheless, in outdoor environments under natural illumination the lighting direction has to be estimated in advance to be able to apply the photometric stereo technique. To solve this issue we used a sundial card to estimate the lighting directions through the angle (with an error of 5 deg) and the length (with an error of 0.5 cm) of the shadow projected by the stick onto this card.

Following from Fig. 5(a) the elevation angle θ and the slant angle φ can be calculated via the expressions

$$\theta = \arctan\left(\frac{R}{L}\right); \quad \varphi = A - 180 \text{ deg}, \tag{15}$$

where R is the length of the shadow, L is the length of the stick and A is the associated angle. This process was used to determine the lighting directions when a light source, e.g., the sun, is located in four different positions to obtain the four images required to apply the recovery algorithm.

Because outdoors we are constrained by solar position we cannot choose elevations and azimuths at will. Barsky and Petrou[10] have shown that the following inequality is sufficient to ensure acceptable illumination configuration

$$\tan \theta_i \tan \theta_j > -\cos(\phi_i - \phi_j), \tag{16}$$

where θ_i is the elevation angle of the ith source and ϕ_i is its tilt angle. This inequality can be loosened or tightened for specific illumination set-ups. Thus we captured four images outdoors at 20-minute intervals to obtain different perceptible sun shadows [Fig. 5(b)], which corresponded to azimuths of 155, 160, 165 and 170 deg, and solar elevations of 62.6, 60.3, 57.7 and 55.4 deg, which ensures that inequality. From the images shown in Fig. 5(b), images number 1 to 4 were selected as the training set to estimate the normals and albedo, and an additional fifth image outside that time interval was used as a test sample. Figure 6 shows examples of the
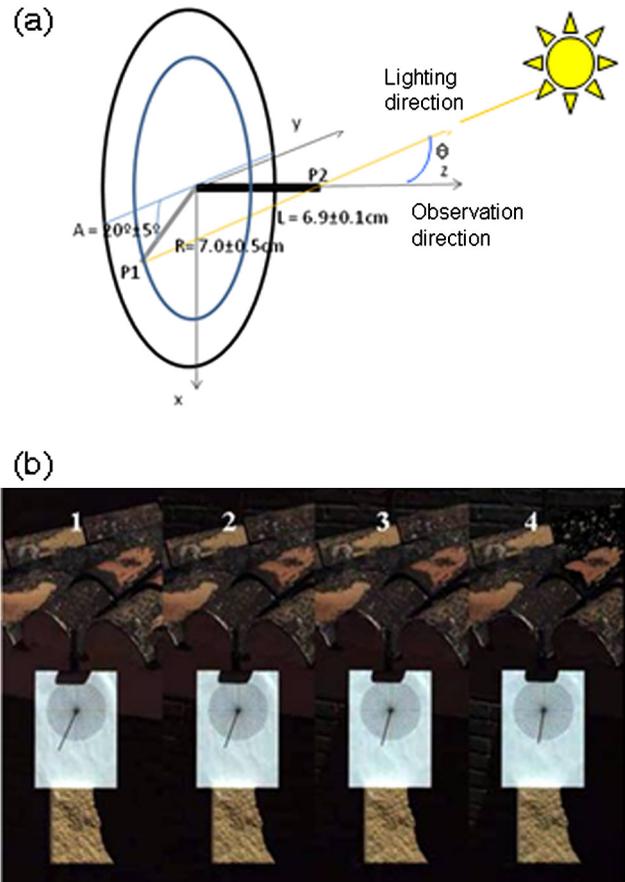

Fig. 5 (a) Example of the geometry of the sundial card used to estimate solar position. (b) Different image captures under natural illumination outdoors.

image rendering from the illuminant-free images for different azimuths and solar elevations. These simulations show very good color accuracy with almost no perceptible differences between the original and the rendered images. But a closer inspection of the color quality indices suggests the contrary, with average color differences of 3 and 8.5 ΔE_{Lab} units for both examples, respectively. The color histograms on the left illustrate the distribution of color errors in the simulations and also give a clear idea of the effect of computing pixel-by-pixel errors in the magnitude of the final error number.

Figure 7 shows the histogram of all CIELab color differences deriving from the illuminant-free outdoor images; the RGB errors are also shown in the inset. On one hand it is clear that the calibration results obtained in the previous section are better than the outdoor results, while on the other hand, clear differences among metrics are obtained. We found an average RGBr_x value of around 8% with an angle error of less than 4 deg and an RGBe_x value of 60 (i.e., less than 1.5% total error). Because the average color difference was around 7 ΔE_{Lab} units our results confirm that so far there is no easy way to assess colorimetric accuracy in the reproduction of color images.[19] Color accuracy can only be assessed on the basis of a pixel-by-pixel calculation, which merely gives approximate overall perceptible differences after averaging out the results for the whole image.
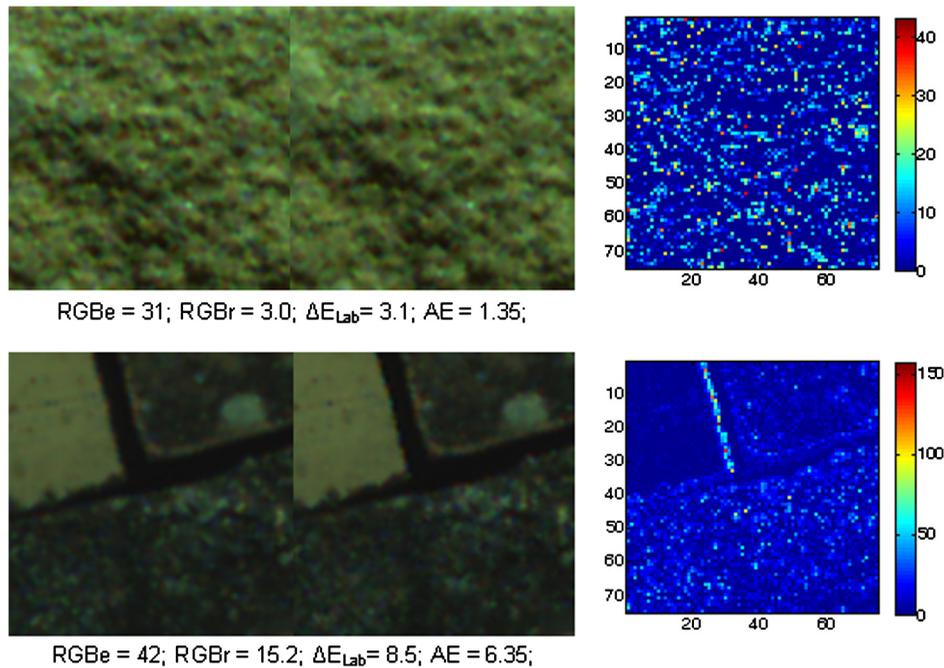
RGBe = 31; RGBr = 3.0; ΔE$_{Lab}$= 3.1; AE = 1.35;

RGBe = 42; RGBr = 15.2; ΔE$_{Lab}$= 8.5; AE = 6.35;

Fig. 6 Examples of albedo recovery (illuminant-free images) outdoors. The first column shows the original images [extracted from the scenes in (a)]; the second column is the rendered image after albedo estimation, and the last column is a 2D histogram of ΔE_{Lab} color differences.

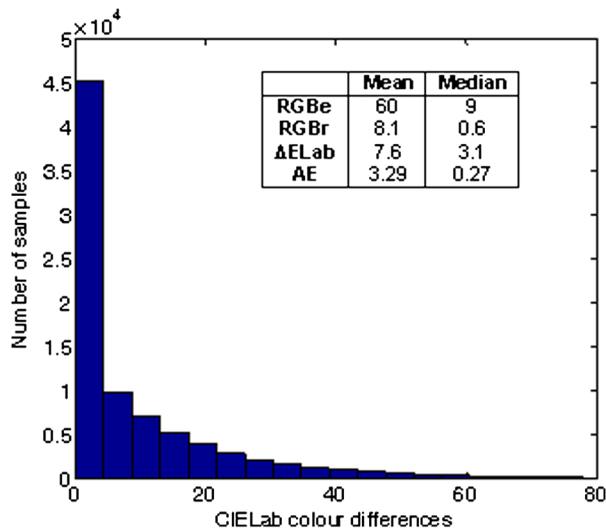|	Mean	Median
RGBe	60	9
RGBr	8.1	0.6
ΔELab	7.6	3.1
AE	3.29	0.27

Fig. 7 Frequency histogram of ΔE_{Lab} color differences obtained for all the rendered images outdoors after albedo estimation. The average and median values for the RGB error (RGBe), the RGB relative error (RGBr), the ΔE_{Lab} color difference and the angle error (AE) are also shown; all the metrics are calculated at each pixel.

4 Discussion and Conclusions

We have described a photometric-stereo device based on a digital RGB camera to obtain illuminant-free color images. Therefore we obtained color images where the RGB color components for each pixel do not depend on the scene illumination. The color of an object depends on the spectral reflectance properties of its surface and the spectral power distribution of the light that illuminates it.[15] Therefore the color of a scene captured by any conventional or digital camera can vary considerably when the ambient light changes.

Most commercial digital cameras incorporate a simple white balance mechanism to solve this problem, but more sophisticated spectral imaging devices either measure the light impinging upon the scene directly or derive some canonical image that is independent of the illuminant conditions. In the latter case, different strategies, usually referred to as color constancy algorithms, are used to obtain color-constant image descriptors.[20] Thus the color albedo recovery could be used an alternative to the color-constancy and/or spectral approaches to solve for the illuminant changes.

The system has been tested indoors using a suitable set of calibration samples. The calibration sample set, composed of chips made of the same material but different colors and textures, was used to calibrate albedos recovered using the photometric-based technique. This color set was used to compare two different approaches, the so-called corrected one, which avoids the effect of shadows and highlights, and the uncorrected one, which ignores this factor. Our results show that the proposed calibration technique is a suitable way of assessing albedos, finding, as it does, very similar values for the reference albedo obtained with both photometric stereo techniques. When comparing albedos obtained from images with complex textures with the respective reference albedo, the photometric stereo technique, which corrects the presence of intensities with non-Lambertian behavior, results in smaller differences. There are in fact other ways of avoiding non-Lambertian behavior, which incorporate extra lights and a hierarchical selection strategy to eliminate the effects of shadows and specularities[16,21] or the combining of various images taken at different exposure times over a high dynamic range.[22] Nevertheless, it is desirable to simplify the problem; the use of our calibration sample set can be used as an alternative way to test albedo recovery without complex devices and/or strategies.

The system was also used outdoors under solar illumination. In this case a sundial device allowed us to estimate the geometry of illumination. Nevertheless, performance was varied when color errors were obtained under these outdoor conditions, probably because of the presence of large complex surfaces. The relative color errors were acceptable with average RGBr_x errors of around 8 but colorimetric accuracy worsened in comparison with the indoor results with CIELab color differences above 5 ΔE_{Lab} units. But the visual significance of colorimetric errors in complex images is still an open question that has not been completely resolved. Previous experiments[19] have found that the observers' ability to discriminate between images needed on average a CIELab color difference of about 2.2, although large variations around this mean for a variety of images were also found. Because the illuminant-free images were obtained here by just using a three-channel RGB digital camera and not a spectral device, the results could be biased by these psychophysical and physical constraints. In addition, albedos were recovered on the basis of the RGB space spanned by the camera and not a human-based color space such as CIELab. Therefore, further studies are needed to analyze what the visual significance of color errors in albedo-free images might be.

Acknowledgments

References

1. E. J. McCartney, *Optics of the Atmosphere: Scattering by Molecules and Particles*, John Wiley & Sons Inc., New York (1976).
2. B. K. Horn and M. J. Brooks, *Shape From Shading* MIT Press, Cambridge, Mass (1989).
3. R. Woodham, "Photometric method for determining surface orientation from multiple images," *Opt. Eng.* **19**(1), 139–144 (1980).
4. E. N. Coleman and R. Jain, "Obtaining 3-dimensional shape of textured and specular surfaces using four source photometry," *Comput. Graph. Image Process.* **18**(4), 309–328 (1982).
5. M. S. Drew, "Photometric stereo without multiple images," *Hum. Vis. Electron. Imag.* **3016**(604), 369–380 (1990).
6. P. H. Christensen and L. G. Shapiro, "Three dimensional shape from color photometric stereo," *Int. J. Comput. Vis.* **13**(2), 213–227 (1994).
7. R. J. Woodham, "*Reflectance Map Techniques for Analyzing Surface Defects in Metal Castings*," TR-457, Artificial Intelligence Laboratory, MIT, Cambridge, Mass (1978).
8. K. Schlüns and O. Witting, "Photometric stereo for non-Lambertian surfaces using color information," *Proc. 5th Int. Conf. Comp. Anal. of Images and Patterns* 444–451 (1993).
9. S. Barsky and M. Petrou, "Color photometric stereo: simultaneous reconstruction of local gradient and color of rough textured surfaces," *Proc. ICCV'01*, Vancouver, Canada, Vol. **2**, 600–605 (2001).
10. S. Barsky and M. Petrou, "The 4-source photometric stereo technique for 3 dimensional surfaces in the presence of highlights and shadows," *IEEE Trans. Pattern Anal. Mach. Intell.* **25**(10), 1239–1252 (2003).
11. C. Plata et al., "Trichromatic red-green-blue camera used for the recovery of albedo and reflectance of rough-textured surfaces under different illumination conditions," *Appl. Opt.* **48**(19), 3643–3653 (2009).
12. C. Plata et al., "Recovering normal vectors and albedo under uncontrolled illumination with an RGB digital camera," *Proc. CGIV 2010*, Joensuu, Finland, **387** (2010).
13. B. Bringier, D. Helbert, and M. Khoudeir, "Photometric reconstruction of a dynamic textured surface from just one color image acquisition," *J. OSA A* **25**(3), 566–574 (2008).
14. F. Chen, G. M. Brown, and M. Song, "Overview of three-dimensional shape measurement using optical methods," *Opt. Eng.* **50**(28), 10–22 (2000).
15. B. A. Wandell, "The synthesis and analysis of color images," *IEEE Trans. Pattern Anal. Mach. Intell.* **9**(1) 2–13 (1987).
16. J. Sun et al., "Object surface recovery using a multi-light photometric stereo technique for non-Lambertian surfaces subject to shadows and specularities," *Image Vis. Comput.* **25**(7, 1050–1057 (2007).
17. C. Plata, S. M. C. Nascimento, and J. L. Nieves, "Accuracy of photometric stereo with textured calibration samples," *Proc. 20th Symp. ICVS*, Braga, Portugal, **123** (2009).
18. http://www.bowensdirect.com.
19. M. A. Aldaba et al., "Visual sensitivity to color errors in images of natural scenes," *Vis. Neurosci.* **23**(3–4), 555–559 (2006).
20. M. Ebner, *Color Constancy*, Wiley, New York (2007).
21. V. Argyrioua, M. Petrou, and S. Barsky, "Photometric stereo with an arbitrary number of illuminants," *Comput. Vis. Image Understand.* **114**(8), 887–900 (2010).
22. M. de Lasarte et al., "Luminance adaptation model for increasing the dynamic range of an imaging system based on a CCD camera," *Opt. Int. LightJ. Electron Opt.* **122**(15), 1367–1372 (2011).

Juan Luis Nieves received his MSc and PhD in physics from the University of Granada, Spain, in 1991 and 1996, respectively. He is currently an associate professor at the Department of Optics in the Science Faculty, University of Granada. At present his research in the Color Imaging Lab at the Department of Optics revolves around computational color vision (color constancy and human visual system processing of spatio-chromatic information), and spectral analysis of color images.

Clara Plata obtained her MSc in physics in 2006 and her PhD in 2009, both at the University of Granada, Spain. She was a research student in the Color Imaging Lab at the Department of Optics from 2003 to 2009 in the field of color imaging.

Eva M. Valero obtained a BD in physics in 1995, and a PhD in 2000, both at the University of Granada, Spain. She has worked at the Department of Optics as an associate professor since 2001. She is a member of the Color Imaging Lab at the University of Granada. Her research interests were initially spatial color vision, and more recently multispectral imaging and color image processing.

Javier Romero is currently full professor in the Science Faculty, University of Granada, Spain, and leads the Color Imaging Lab at the Department of Optics. The research at the Color Imaging Lab covers different topics, from color and spectral imaging to atmospheric optics and education in optics.